A Study of Task-Space Path-Velocity Control for Torque-Limited Redundant Manipulators under Uncertainties

Jia, Zheng; Karayiannidis, Yiannis; Olofsson, Björn

Published in:
2025 European Control Conference (ECC)

DOI:
10.23919/ECC65951.2025.11187049

2025

A Study of Task-Space Path-Velocity Control for Torque-Limited Redundant Manipulators under Uncertainties

Zheng Jia[1], Yiannis Karayiannidis[1], and Björn Olofsson[1,2]

***Abstract*— This paper addresses the time-optimal path-tracking problem for redundant manipulators. By integrating path-velocity control into existing task-space robot controllers, the task-space motion can be dynamically scaled to satisfy the torque constraint under both kinematic and dynamic uncertainties. Numerical simulations and experiments demonstrate that trajectory feasibility and path-tracking accuracy of the task-space controllers can be significantly improved by integrating path-velocity control. In addition, the nullspace motion of redundant manipulators can be exploited to further improve the performance by tracking the approximate time-optimal joint trajectory associated with the tasks in nullspace.**

I. Introduction

Accurate and fast movement of the robot end-effector can be achieved by controlling the manipulator to follow the desired joint angles as quickly as possible [1]. However, when a robot operates while grasping a tool with approximate dimensions and an uncertain position, and the control objective is focused on the tool rather than the gripper or flange, kinematic uncertainty arises. Task-space control with workspace sensing addresses the challenge of accurate movement in the presence of kinematic uncertainty [2]–[4]. However, the movement speed of manipulators is always constrained by the torque limits of the actuators. Kinematic or dynamic uncertainties may cause the planned fast motions to be unrealizable by the task-space controller. In applications where a desired path in task space is prescribed, violation of the torque constraint implies degraded performance of feedback control and path deviation [5]–[9].

Trajectory scaling can be adopted to solve the problem of constraint satisfaction in the presence of uncertainties [5]–[11]. In particular, Path-Velocity Control (PVC) focuses on ensuring trajectory feasibility of time-optimal motions with respect to torque constraints under dynamic uncertainty [5]–[8]. An intuitive way to address violations of the torque constraint is to apply PVC to task-space control. However, PVC is originally designed for the joint controllers of manipulators (assuming exact knowledge of kinematics). Thus, it is of interest to study its applicability to task-space controllers and the resulting performance for improving trajectory feasibility and task-space accuracy in the presence of kinematic and dynamic uncertainties. For redundant manipulators, with task-space control objectives, controlling the nullspace motion is a common approach. As a degree of freedom, the redundancy has been exploited for many applications [12]–[16]. Its effect on trajectory scaling and control performance of the combined method is studied in this paper.

The primary contribution of this paper is the study and evaluation of the concept of applying PVC [7], [8] to improve the performance of task-space control with respect to the torque constraint. Our findings indicate that the performance of the task-space control can be significantly improved with the integration of PVC, and further enhanced by tracking the joint trajectory associated with the tasks in nullspace.

This paper is organized as follows. Section II provides a concise review of the manipulator dynamics and kinematics. Section III formulates the problems of interest. Section IV describes task-space control methods with redundancy resolution. Path-velocity control and its integration into the task-space controller are described in Section V. The simulation and experimental results are presented in Section VI and Section VII. The paper concludes with Section VIII, where we summarize our findings and suggest directions for future research.

II. Robot Kinematics and Dynamics

Consider an n-dof manipulator with its joint variable denoted by $\boldsymbol{q}$ and end-effector pose described by

$$\boldsymbol{H}_e(\boldsymbol{q}) = \begin{bmatrix} \boldsymbol{R}_e & \boldsymbol{p}_e \\ 0 & 1 \end{bmatrix}, \tag{1}$$

where $\boldsymbol{R}_e$ and $\boldsymbol{p}_e$ represent the end-effector orientation and position, respectively. The end-effector velocity $\boldsymbol{v}_e$ is

$$\boldsymbol{v}_e = \begin{bmatrix} \dot{\boldsymbol{p}}_e \\ \boldsymbol{\omega}_e \end{bmatrix} = \boldsymbol{J}(\boldsymbol{q})\dot{\boldsymbol{q}}, \tag{2}$$

with $\boldsymbol{J}(\boldsymbol{q}) \in \mathbb{R}^{6\times n}$ being the geometric Jacobian of the manipulator, which maps joint velocities $\dot{\boldsymbol{q}}$ to the linear velocity $\dot{\boldsymbol{p}}_e$ and angular velocity $\boldsymbol{\omega}_e$ of the end-effector. The dynamics of the manipulator is described by [17], [18]

$$\boldsymbol{B}(\boldsymbol{q})\ddot{\boldsymbol{q}} + \boldsymbol{n}(\boldsymbol{q}, \dot{\boldsymbol{q}}) = \boldsymbol{\tau}, \tag{3}$$

where $\boldsymbol{B}(\boldsymbol{q})$ is the inertia matrix, $\boldsymbol{n}(\boldsymbol{q}, \dot{\boldsymbol{q}})$ are the Coriolis and gravity vectors, and $\boldsymbol{\tau}$ denotes the joint torque. In this paper, the following torque constraint is primarily considered

$$\boldsymbol{\tau}_{\min} \leq \boldsymbol{\tau} \leq \boldsymbol{\tau}_{\max}. \tag{4}$$

This work was supported by the ELLIIT Strategic Research Area, and partially supported by the Wallenberg AI, Autonomous Systems and Software Program (WASP) funded by the Knut and Alice Wallenberg Foundation.

[1]Zheng Jia, Yiannis Karayiannidis, and Björn Olofsson are with the Department of Automatic Control, Lund University, Sweden, {zheng.jia, yiannis, bjorn.olofsson}@control.lth.se.

[2]Björn Olofsson is also with the Division of Vehicular Systems, Department of Electrical Engineering, Linköping University, Sweden.

III. Problem Formulation

The task-space control problem considered in this paper is that the end-effector of a redundant manipulator should follow a desired pose

$$\boldsymbol{H}_d(s) = \begin{bmatrix} \boldsymbol{R}_d(s) & \boldsymbol{p}_d(s) \\ 0 & 1 \end{bmatrix} \tag{5}$$

parameterized by the path coordinate $s \in [0, 1]$, in the shortest possible time, while not violating the torque constraint (4). The variable $\boldsymbol{p}_d(s)$ defines the geometric path in Cartesian space, and $\boldsymbol{R}_d(s)$ describes the end-effector orientation along the path.

The path itself specifies only the geometry of the task. To follow $\boldsymbol{H}_d(s)$ as fast as possible, a time-optimal path-tracking problem needs to be solved first. One practical solution is to divide it into two sub-problems: first, solving for an inverse kinematics solution $\boldsymbol{q}_d(s)$, and second, determining a time-optimal solution $s(t)$ for $\boldsymbol{q}_d(s)$ [19]–[24]. Then, the task of following a desired configuration $\boldsymbol{H}_d(s)$ can either be addressed by a task-space controller following $\boldsymbol{H}_d(s(t))$, or a joint-space controller following $\boldsymbol{q}_d(s(t))$.

Two challenges are faced when using a joint-space controller to follow $\boldsymbol{H}_d(s)$. First, in the presence of kinematic uncertainty, only an approximate solution $\hat{\boldsymbol{q}}_d(s)$ is obtained, which makes it difficult to precisely follow $\boldsymbol{H}_d(s)$. Second, minimum-time solutions in joint space always saturate at least one actuator [22]–[24], which leaves no more torque available to compensate for dynamic uncertainty. One effective approach to address this problem is to apply PVC to dynamically scale down the nominal minimum-time joint motions [5]–[8].

Alternatively, a task-space controller with external sensors may be adopted to tackle the first challenge [2]–[4]. An intuitive way to approach the second challenge may be the application of the path-velocity control [7], [8] to the task-space controller, with an additional complexity because of the redundancy. Therefore the objective of this paper is to:

1) Study and evaluate the performance of the combined task-space and path-velocity controller (TS-PVC).
2) Investigate and compare the performance of TS-PVC with different nullspace control designs.

IV. Task-Space Control

A. Definition of Task-Space Error

The problem of following the desired pose (5) is formulated in a local task frame $\{a\}$ attached to the path $\boldsymbol{p}_d(s)$, with its orientation denoted by $\boldsymbol{R}_a(s)$. Let $\Delta\boldsymbol{p} = \boldsymbol{p}_d(t) - \boldsymbol{p}_e(t)$, $\{\eta_{de}, {}^e\boldsymbol{\epsilon}_{de}\}$ be the unit quaternion extracted from the rotation difference $\boldsymbol{R}_{ed} = \boldsymbol{R}_e^T\boldsymbol{R}_d$, and $\Delta\boldsymbol{\omega} = \boldsymbol{\omega}_d(t) - \boldsymbol{\omega}_e(t)$, then the task-space position, orientation, and angular velocity error are defined as

$$^a\Delta\boldsymbol{p} = \boldsymbol{R}_a^T\Delta\boldsymbol{p}, \tag{6}$$

$$^e\Delta\boldsymbol{o} = {}^e\boldsymbol{\epsilon}_{de}, \tag{7}$$

$$^e\Delta\boldsymbol{\omega} = \boldsymbol{R}_e^T\Delta\boldsymbol{\omega}. \tag{8}$$

The unit quaternion is chosen because it is representation-singularity free and it is straightforward to parameterize the desired angular velocity and acceleration as $\boldsymbol{\omega}_d(t) = \boldsymbol{\omega}_d(s)\dot{s}$ and $\dot{\boldsymbol{\omega}}_d(t) = \boldsymbol{\omega}_d(s)\ddot{s} + \boldsymbol{\omega}'_d(s)\dot{s}^2$ in $(s, \dot{s}, \ddot{s})$ for quaternion-based orientation control, where the notation $(\cdot)'$ denotes differentiation with respect to s.

B. Task-Space Control with Redundancy Resolution

Several task-space control methods with redundancy resolution exist. A common choice is the Cartesian inverse-dynamics control in combination with nullspace control [25], [26]

$$\boldsymbol{\tau} = \hat{\boldsymbol{B}}\left[\hat{\boldsymbol{J}}_{\boldsymbol{Q}}^{\dagger}\left(\boldsymbol{u} - \dot{\hat{\boldsymbol{J}}}\dot{\boldsymbol{q}}\right) + \left(\boldsymbol{I} - \hat{\boldsymbol{J}}_{\boldsymbol{Q}}^{\dagger}\hat{\boldsymbol{J}}\right)\ddot{\boldsymbol{q}}_n\right] + \hat{\boldsymbol{n}}, \tag{9}$$

where $\boldsymbol{u}$ and $\ddot{\boldsymbol{q}}_n$ are the resolved-acceleration and nullspace control input. $\hat{\boldsymbol{J}}_{\boldsymbol{Q}}^{\dagger} = \boldsymbol{Q}^{-1}\hat{\boldsymbol{J}}^T(\hat{\boldsymbol{J}}\boldsymbol{Q}^{-1}\hat{\boldsymbol{J}}^T)^{-1}$ is a pseudo-inverse of $\hat{\boldsymbol{J}}$, weighted by a positive definite matrix $\boldsymbol{Q}$. The dynamically consistent pseudo-inverse $\boldsymbol{Q} = \hat{\boldsymbol{B}}(\boldsymbol{q})$ is chosen in this paper [27]. In (9) and the remainder of this paper, the notation $\hat{(\cdot)}$ refers to the estimated quantities. When there is no estimation error in manipulator parameters, (9) transforms the dynamics (3) to $\dot{\boldsymbol{v}}_e = \boldsymbol{u}$.

C. Inverse Dynamics Control

A desired task-space error dynamics can be specified as [18], [28]

$$^a\Delta\ddot{\boldsymbol{p}} + \boldsymbol{D}_p{}^a\Delta\dot{\boldsymbol{p}} + \boldsymbol{K}_p{}^a\Delta\boldsymbol{p} = \boldsymbol{0}, \tag{10}$$

$$^e\Delta\dot{\boldsymbol{\omega}} + \boldsymbol{D}_o{}^e\Delta\boldsymbol{\omega} + \boldsymbol{K}_o{}^e\Delta\boldsymbol{o} = \boldsymbol{0}, \tag{11}$$

where $\boldsymbol{K}_p$ and $\boldsymbol{K}_o$ are stiffness matrices, and $\boldsymbol{D}_p$ and $\boldsymbol{D}_o$ are damping matrices. Substituting (6)–(8) in (10)–(11) and using $\dot{\boldsymbol{v}}_e = \boldsymbol{u}$, the input $\boldsymbol{u}$ can be computed as

$$\begin{aligned}\boldsymbol{u} = &\begin{bmatrix} \ddot{\boldsymbol{p}}_d \\ \dot{\boldsymbol{\omega}}_d \end{bmatrix} + \begin{bmatrix} \boldsymbol{R}_a\ddot{\boldsymbol{R}}_a^T\Delta\boldsymbol{p} \\ 0 \end{bmatrix} + \begin{bmatrix} 2\boldsymbol{R}_a\dot{\boldsymbol{R}}_a^T\Delta\dot{\boldsymbol{p}} \\ \boldsymbol{R}_e\dot{\boldsymbol{R}}_e^T\Delta\boldsymbol{\omega} \end{bmatrix} \\ &+ \begin{bmatrix} \boldsymbol{R}_a\left(\boldsymbol{D}_p{}^a\Delta\dot{\boldsymbol{p}} + \boldsymbol{K}_p{}^a\Delta\boldsymbol{p}\right) \\ \boldsymbol{R}_e\left(\boldsymbol{D}_o{}^e\Delta\boldsymbol{\omega} + \boldsymbol{K}_o{}^e\Delta\boldsymbol{o}\right) \end{bmatrix}.\end{aligned} \tag{12}$$

D. Nullspace Control

Next, the nullspace control input $\ddot{\boldsymbol{q}}_n$ is chosen as [12]

$$\ddot{\boldsymbol{q}}_n = \ddot{\boldsymbol{q}}_0 + \boldsymbol{D}_q(\dot{\boldsymbol{q}}_0 - \dot{\boldsymbol{q}}) + \boldsymbol{K}_q(\boldsymbol{q}_0 - \boldsymbol{q}) \tag{13}$$

for simplicity, where $\boldsymbol{D}_q$ and $\boldsymbol{K}_q$ are the damping and stiffness matrices, respectively. The reference $\boldsymbol{q}_0$ can be set to a preferred joint equilibrium, e.g., the center of the joint-angle limits, or to an estimated nominal joint trajectory $\hat{\boldsymbol{q}}_d(t)$. In general, nullspace trajectories are not necessary for the task-space control of redundant manipulators. However, it will be shown in Section VI and Section VII that tracking the approximate joint trajectory in the nullspace reduces the path traversal time and the risk of inadmissible path acceleration, compared to either tracking a virtual equilibrium or using only the nullspace damping control. While nullspace control has a significant influence on the performance of time-optimal path tracking, provided that it is path-parameterized, its specific form does not hinder its integration with path-velocity control.

V. Task-space Path Velocity Control

This section applies and integrates path-velocity control [5]–[8] into the task-space controller (9). Let $\boldsymbol{v}_d = \boldsymbol{T}_d(s)\dot{s}$ denote the task-space velocity, where $\boldsymbol{T}_d(s) = \left[\begin{smallmatrix} \boldsymbol{p}'_d(s) \\ \boldsymbol{\omega}_d(s) \end{smallmatrix}\right]$. The acceleration input $\boldsymbol{u}$ in (12) can be parameterized as a function of $(s, \dot{s}, \ddot{s})$ according to

$$\begin{aligned}\boldsymbol{u} = &\left(\boldsymbol{T}_d + \begin{bmatrix} \boldsymbol{R}_a \left(\boldsymbol{R}'_a\right)^T \Delta\boldsymbol{p} \\ 0 \end{bmatrix}\right) \ddot{s} \\ &+ \left(\boldsymbol{T}'_d + \begin{bmatrix} \boldsymbol{R}_a \left(\boldsymbol{R}''_a\right)^T \Delta\boldsymbol{p} \\ 0 \end{bmatrix}\right) \dot{s}^2 \\ &+ \begin{bmatrix} 2\boldsymbol{R}_a \dot{\boldsymbol{R}}_a^T \Delta\dot{\boldsymbol{p}} \\ \boldsymbol{R}_e \dot{\boldsymbol{R}}_e^T \Delta\boldsymbol{\omega} \end{bmatrix} \\ &+ \begin{bmatrix} \boldsymbol{R}_a \left(\boldsymbol{D}_p{}^a \Delta\dot{\boldsymbol{p}} + \boldsymbol{K}_p{}^a \Delta\boldsymbol{p}\right) \\ \boldsymbol{R}_e \left(\boldsymbol{D}_o{}^e \Delta\boldsymbol{\omega} + \boldsymbol{K}_o{}^e \Delta\boldsymbol{o}\right) \end{bmatrix} \\ &= \boldsymbol{\pi}_1(\boldsymbol{q}, s)\ddot{s} + \boldsymbol{\pi}_2(\boldsymbol{q}, \dot{\boldsymbol{q}}, s, \dot{s}). \end{aligned} \tag{14}$$

The nullspace control (13) can similarly be parameterized as

$$\begin{aligned}\ddot{\boldsymbol{q}}_n &= \hat{\boldsymbol{q}}'_d \ddot{s} + \hat{\boldsymbol{q}}''_d \dot{s}^2 + \boldsymbol{D}_q \left(\hat{\boldsymbol{q}}'_d \dot{s} - \dot{\boldsymbol{q}}\right) + \boldsymbol{K}_q \left(\hat{\boldsymbol{q}}_d - \boldsymbol{q}\right) \\ &= \boldsymbol{\Gamma}_1(s)\ddot{s} + \boldsymbol{\Gamma}_2\left(\boldsymbol{q}, \dot{\boldsymbol{q}}, s, \dot{s}\right). \end{aligned} \tag{15}$$

The path-parameterized task-space control with redundancy resolution (9) can now be rewritten in the following form

$$\boldsymbol{\tau} = \boldsymbol{\beta}_1\left(\boldsymbol{q}, s\right)\ddot{s} + \boldsymbol{\beta}_2\left(\boldsymbol{q}, \dot{\boldsymbol{q}}, s, \dot{s}\right) \tag{16}$$

where

$$\boldsymbol{\beta}_1 = \hat{\boldsymbol{B}}\left(\hat{\boldsymbol{J}}_{\boldsymbol{Q}}^{\dagger}\boldsymbol{\pi}_1 + \boldsymbol{P}\boldsymbol{\Gamma}_1\right), \tag{17}$$

$$\boldsymbol{\beta}_2 = \hat{\boldsymbol{B}}\left(\hat{\boldsymbol{J}}_{\boldsymbol{Q}}^{\dagger}\left(\boldsymbol{\pi}_2 - \dot{\hat{\boldsymbol{J}}}\dot{\boldsymbol{q}}\right) + \boldsymbol{P}\boldsymbol{\Gamma}_2\right) + \hat{\boldsymbol{n}} \tag{18}$$

and $\boldsymbol{P} = \left(\boldsymbol{I} - \hat{\boldsymbol{J}}_{\boldsymbol{Q}}^{\dagger}\hat{\boldsymbol{J}}\right)$.

With a task-space controller parameterized in $(s, \dot{s}, \ddot{s})$, PVC aims to compute a feasible path acceleration $\ddot{s}$ online to satisfy the torque constraint (4)

$$\boldsymbol{\tau}_{\min} \leq \boldsymbol{\beta}_1\left(\boldsymbol{q}, s\right)\ddot{s} + \boldsymbol{\beta}_2\left(\boldsymbol{q}, \dot{\boldsymbol{q}}, s, \dot{s}\right) \leq \boldsymbol{\tau}_{\max}. \tag{19}$$

The constraint (19) can be transformed into a path acceleration constraint given by

$$\ddot{s}_{\min}\left(\boldsymbol{\beta}_1, \boldsymbol{\beta}_2\right) \leq \ddot{s} \leq \ddot{s}_{\max}\left(\boldsymbol{\beta}_1, \boldsymbol{\beta}_2\right), \tag{20}$$

where $\ddot{s}_{\min}$ and $\ddot{s}_{\max}$ are dynamic path-acceleration bounds, and their computation is detailed in [5]–[8]. Introducing $\ddot{s}_r$ and $\dot{s}_r$ as the nominal solution of the time-optimal path-tracking problem [23], γ as a scaling parameter, $0 \leq \gamma \leq 1$, α as a feedback control gain, k_γ as a positive tuning parameter, the desired path acceleration $\ddot{s}$ computed by PVC is [5]–[8]

$$\ddot{s} = \mathrm{sat}\left(u_r; \ddot{s}_{\min}(\boldsymbol{\beta}_1, \boldsymbol{\beta}_2), \ddot{s}_{\max}(\boldsymbol{\beta}_1, \boldsymbol{\beta}_2)\right), \tag{21}$$

$$u_r = \gamma^2 \ddot{s}_r + \frac{\alpha}{2}\left(\gamma^2 \dot{s}_r^2 - \dot{s}^2\right), \tag{22}$$

$$\dot{\gamma} = \begin{cases} k_\gamma \dot{s}(\dot{s}/\dot{s}_r - \gamma), & \gamma\dot{s}_r \geq \dot{s} \\ 0, & \gamma\dot{s}_r < \dot{s} \end{cases} \tag{23}$$

where $\mathrm{sat}\left(\cdot; \ddot{s}_{\min}, \ddot{s}_{\max}\right)$ is the saturation function with $\ddot{s}_{\min}$ and $\ddot{s}_{\max}$ as its lower and upper bounds. The torque constraint (19) can be satisfied whenever $\ddot{s}_{\min} \leq \ddot{s}_{\max}$. The task-space controller with integrated path-velocity control is obtained by substituting (21) into (16).

VI. Simulation Results

TS-PVC is first evaluated on a simulated Franka Emika Panda Robot in the Algoryx Dynamics simulation environment[1] (AGX), based on the parameters identified in [29]. TS-PVC is implemented using the open-source Robotics Toolbox for Python (RTB) [30]. The inverse kinematics problem is solved using the Levenberg-Marquardt Numerical Inverse Kinematics Solver provided by RTB, and the computation of $\ddot{s}_r(s)$ and $\dot{s}_r(s)$ is performed in MATLAB using the method in [23]. Both the simulation time step and the control interval are set to 1 ms.

The task is to track a circular path with the end-effector in Cartesian space. The position is parameterized as $\boldsymbol{p}_d(s) = [0.384 + 0.2\cos(2\pi s), 0.2\sin(2\pi s), 0.413]^{\mathrm{T}}$ m. The desired end-effector orientation is $\boldsymbol{R}_d(s) = \mathrm{rot}(x, \pi/4)$, i.e., a constant rotation of $\pi/4$ about the x-axis. The orientation of the moving task frame $\{a\}$ attached to the circle is $\boldsymbol{R}_a(s) = \mathrm{rot}(z, 2\pi s)$.

Two simulation scenarios are defined to evaluate the performance of TS-PVC. In the first scenario, kinematic uncertainty between the model and the simulated robot is introduced by increasing the length of each link in the model by 5%. An approximate joint path $\hat{\boldsymbol{q}}_d(s)$ is then obtained and the time-optimal path-tracking problem is solved, which results in a nominal path traversal time $T^{\mathrm{nom}} = 0.586$ s. In the second scenario, both kinematic and dynamic uncertainties are involved simultaneously, where the dynamic uncertainty is introduced by increasing each link mass of the simulated robot by 10%. Within both scenarios, task-space control (16) with three nullspace control designs in the form of (13) are compared and here referred to as Controller 1–3:

1) Controller 1: tracking a virtual equilibrium in nullspace. For each joint i, the equilibrium is set to the center of its joint limits as $\boldsymbol{q}_0^i = 0.5\left(\boldsymbol{q}_{\min}^i + \boldsymbol{q}_{\max}^i\right)$,
$$\ddot{\boldsymbol{q}}_n = -\boldsymbol{D}_q\dot{\boldsymbol{q}} + \boldsymbol{K}_q(\boldsymbol{q}_0 - \boldsymbol{q}), \tag{24}$$
2) Controller 2: damping the nullspace velocity,
$$\ddot{\boldsymbol{q}}_n = -\boldsymbol{D}_q\dot{\boldsymbol{q}}, \tag{25}$$
3) Controller 3: tracking the approximate joint trajectory in nullspace,
$$\ddot{\boldsymbol{q}}_n = \ddot{\hat{\boldsymbol{q}}}_d + \boldsymbol{D}_q(\dot{\hat{\boldsymbol{q}}}_d - \dot{\boldsymbol{q}}) + \boldsymbol{K}_q(\hat{\boldsymbol{q}}_d - \boldsymbol{q}) \tag{26}$$

Controller 1–3 can be viewed as representative examples of position-based, damping-based, and trajectory-based nullspace control strategies, respectively. For each controller, the parameter k_γ is incrementally tuned from 0 to 3000, and its minimum value that ensures τ_1–τ_7 to be within their limits is selected. Since $\boldsymbol{K}_q, \boldsymbol{D}_q$ for nullspace control influence not only the evolution of the joint vari-

[1]April 9, 2025. Available: https://www.algoryx.se/agx-dynamics/

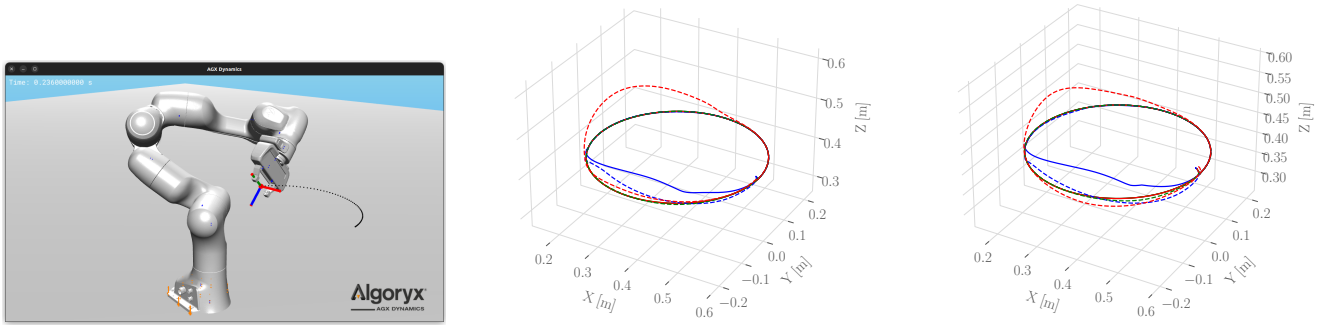

(a) Panda in AGX Dynamics (b) Length error (5%) (c) Length error (5%) and mass error (10%)

Fig. 1: Simulated Panda robot tracking a circular path in Cartesian space. The solid black line represents the reference path. The blue, green, and red lines represent the resulting positions with Controller 1, Controller 2, and Controller 3, respectively. Solid lines represent controllers with PVC, while dashed lines represent controllers without PVC. The lines for the reference path and the signals from Controller 2–3+PVC overlap.

able $\boldsymbol{q}$, but also increase the total joint torque at higher gains, their smallest values are selected, provided that the joint-angle limits for $\boldsymbol{q}$ are not violated. All controllers have the same $\boldsymbol{K}_p = \text{diag}([64\pi^2, 64\pi^2, 64\pi^2])$, $\boldsymbol{D}_p = \text{diag}([16\pi, 16\pi, 16\pi])$, $\boldsymbol{K}_o = \text{diag}([36\pi^2, 36\pi^2, 36\pi^2])$, and $\boldsymbol{D}_o = \text{diag}([12\pi, 12\pi, 12\pi])$. Their values are selected to impose critically damped dynamics in (10)–(11). Key metrics for performance evaluation include the root mean squared error (RMSE) and the maximum path-tracking error $e_{\max} = \max_{0\le s\le 1}\|e(s)\|_2$ for position and orientation, path traversal time T, and the percentage increase $\Delta P = (T - T^{\text{nom}})/T^{\text{nom}}$. In particular, the orientation error is measured by the angle $\phi_{de} = 2\arccos(\eta_{de})$, where $\phi_{de} \in [0, 2\pi]$.

A. Kinematic Uncertainty

When kinematic uncertainty is present, noticeable path deviation can occur during the path tracking, as shown in Fig. 1b. This deviation is caused by torque constraint violations. As seen in Fig. 2a–Fig. 2c, tracking $\dot{s}_r$ requires more torques than their respective limits. On the other hand, Fig. 2d–Fig. 2f show that the integration of PVC eliminates the constraint violation for Controller 2 and 3, at the cost of a longer path traversal time (see the values in bold font for T and ΔP in Table I).

As a result, the overall path-tracking accuracy improves for both Controller 2 and 3 (see the values in bold font for the positional error of Controller 3, before and after integrating PVC, in Table I). Additionally, Controller 3+PVC achieves a higher average path traversal speed $\dot{s}$, shorter traversal time, and higher torque utilization than Controller 2+PVC.

It is also observed that for Controller 1+PVC, the constraint violation can only be eliminated at the beginning of the path tracking, even when $\dot{s}$ is scaled down significantly. This may indicate that tracking a fixed equilibrium in nullspace causes the joint variable $\boldsymbol{q}$ to reach a configuration that is difficult for Cartesian movement.

B. Kinematic and Mass Uncertainties

When mass uncertainty is introduced, the path deviation for Controller 2 and 3 can again be reduced by PVC, but with increased tracking error and path traversal time, comparing RMSE, $e_{\max}$, and T of Controller 2–3+PVC in Table I and Table II (see the values in bold font for Controller 3+PVC). This is expected because model uncertainty increases and the path acceleration capability is reduced with a higher link mass. The minimum value of k_γ for Controller 2+PVC increases from 750 to 2200 with the additional mass uncertainty, whereas the value of k_γ remains unchanged for Controller 3+PVC.

TABLE I: Simulation results of time-optimal tracking of a circular path under 5% error in link length. Root Mean Squared Error for Position [mm] and Angle [rad], Maximum Path-Tracking Error for Position [mm] and Angle [rad], Path Traversal Time [s], Percent Increase [-] and Parameters.

Length error (5%)	RMSE		$e_{\max}$		T	ΔP	α	k_γ	$\boldsymbol{K}_q$	$\boldsymbol{D}_q$
	Position	Angle	Position	Angle						
Controller 1	11.792	0.078	37.852	0.210	0.586	0	20	-	100	20
Controller 2	1.136	0.024	3.349	0.074	0.586	0	20	-	-	100
Controller 3	**30.468**	0.393	**69.540**	0.882	0.586	0	20	-	100	20
Controller 1+PVC	24.686	0.260	70.016	0.579	0.767	30.9%	20	3000	100	20
Controller 2+PVC	0.562	0.003	0.871	0.006	**0.642**	**9.6%**	20	750	-	100
Controller 3+PVC	**0.598**	0.004	**0.995**	0.007	**0.625**	**6.7%**	20	12	100	20

TABLE II: Simulation results of time-optimal tracking of a circular path under 5% error in link length and 10% error in link mass. Root Mean Squared Error for Position [mm] and Angle [rad], Maximum Path-Tracking Error for Position and Angle [rad], Path Traversal Time [s], Percent Increase [-] and Parameters.

Length error (5%) Mass error (10%)	RMSE		$e_{\max}$		T	ΔP	α	k_γ	$\boldsymbol{K}_q$	$\boldsymbol{D}_q$
	Position	Angle	Position	Angle						
Controller 1	8.732	0.100	23.757	0.236	0.586	0	20	-	100	20
Controller 2	2.504	0.067	7.696	0.193	0.586	0	20	-	-	100
Controller 3	22.373	0.317	54.840	0.748	0.559	0	20	-	100	20
Controller 1+PVC	26.252	0.283	72.520	0.620	0.779	32.9%	20	3000	100	20
Controller 2+PVC	0.648	0.004	0.996	0.006	0.674	15.0%	20	2200	-	100
Controller 3+PVC	**0.677**	0.004	**1.073**	0.007	**0.669**	**14.2%**	20	12	100	20

VII. Experimental Results

The performance of TS-PVC is further evaluated on the Franka Emika Panda robot[2]. The inverse kinematics and time-optimal path-tracking problems are solved assuming a tool center point (TCP) offset of 103.4 mm along the z-axis of the flange frame. To introduce kinematic uncertainty, the actual TCP offset is increased from 103.4 mm to 185 mm. The position measurement $\boldsymbol{p}_e$ of the actual TCP is obtained using

[2]April 9, 2025. Available: https://frankaemika.github.io/docs/

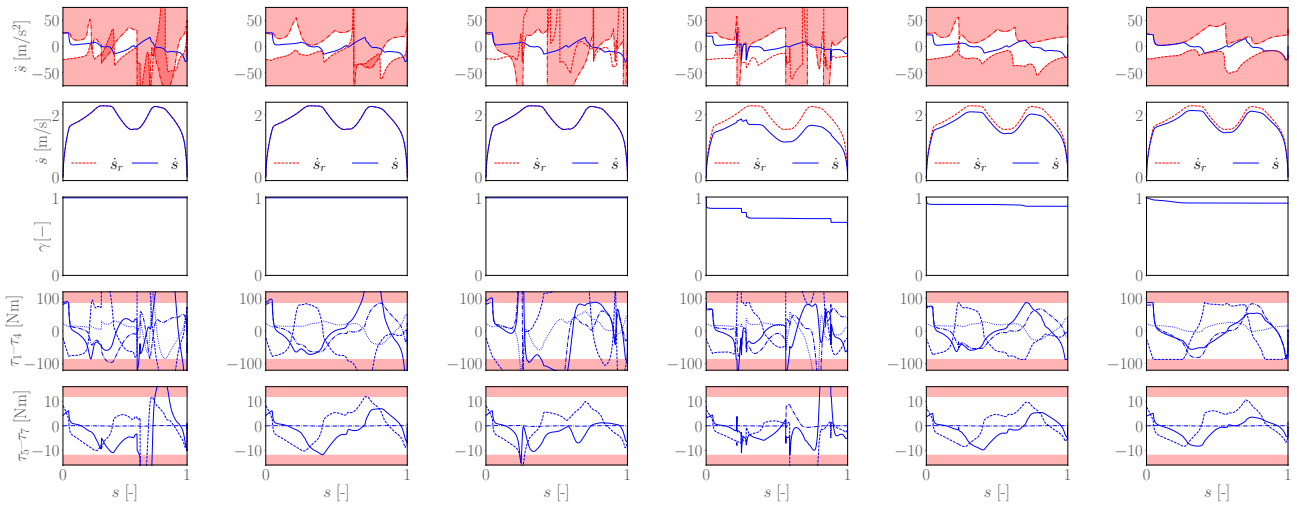

(a) Controller 1 (b) Controller 2 (c) Controller 3 (d) Controller 1+PVC (e) Controller 2+PVC (f) Controller 3+PVC

Fig. 2: Time-optimal path-tracking in simulation of a circular path under 5% error in link length. Within each subplot, the signals from top to bottom are path acceleration $\ddot{s}$, path velocity $\dot{s}$, joint torques τ_1–τ_4 and τ_5–τ_7. The red areas indicate inadmissible regions for the signals.

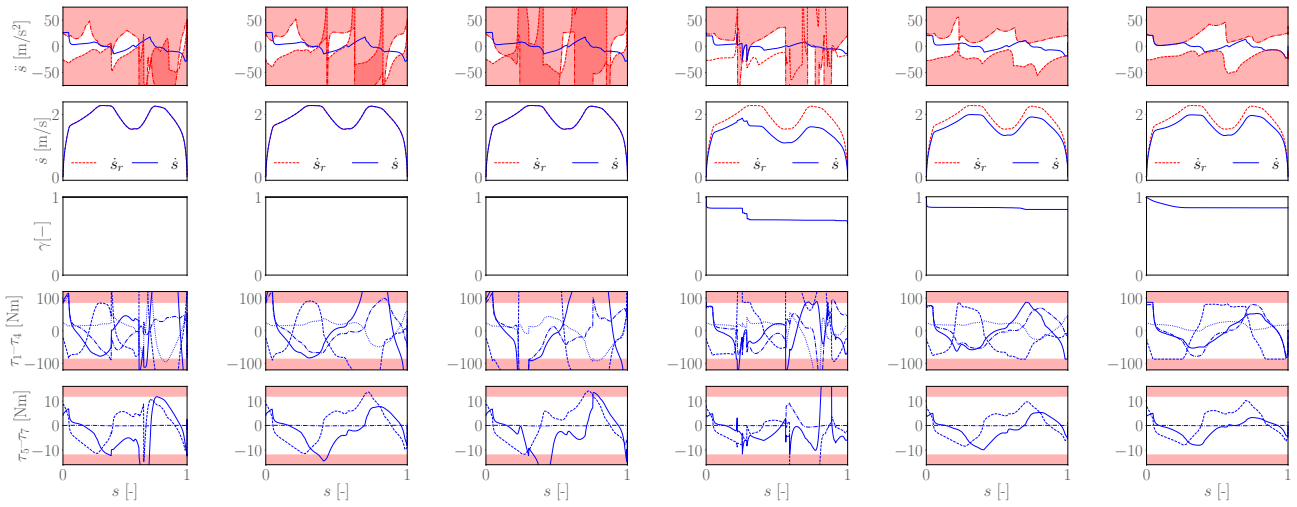

(a) Controller 1 (b) Controller 2 (c) Controller 3 (d) Controller 1+PVC (e) Controller 2+PVC (f) Controller 3+PVC

Fig. 3: Time-optimal path-tracking in simulation of a circular path under 5% error in link length and 10 % error in link mass. Within each subplot, the signals from top to bottom are path acceleration $\ddot{s}$, path velocity $\dot{s}$, joint torques τ_1–τ_4 and τ_5–τ_7. The red areas indicate inadmissible regions for the signals.

forward kinematics. The tuning of the parameter k_γ follows the same procedure as in the simulations.

A. Results

The experiments of tracking $(\ddot{s}_r, \dot{s}_r)$ by Controller 1–3 without PVC cannot be completed because the joint velocity limits are violated during the path tracking and the motion is stopped at $s \approx 0.34$. The signals recorded up to this point are shown in Fig. 4a–Fig. 4c. Since the joint configuration $\boldsymbol{q}$ does not follow the nominal inverse kinematic solution $\hat{\boldsymbol{q}}_d$ (at least not precisely under kinematic uncertainty), realizing the nominal task-space velocity $\boldsymbol{T}_d \dot{s}_r$ may require $\dot{\boldsymbol{q}}$ to exceed the joint velocity limits. Moreover, Fig. 4a–Fig. 4c show that the torque constraint is violated at the beginning of the path tracking, which indicates that the nominal solution $(\ddot{s}_r, \dot{s}_r)$ is infeasible with respect to the torque constraint under combined kinematic and mass uncertainties.

The path-tracking results for Controller 1–3+PVC are shown in Fig. 5. Fig. 4d–Fig. 4f show that the torque constraint is satisfied for all three controllers. In particular, γ is gradually adapted to a value such that tracking $\gamma \dot{s}_r$ is feasible for the entire path tracking. The fluctuations observed in τ_3 can be attributed to the noisy measurements of $\dot{\boldsymbol{q}}$ in (16). As seen in Fig. 4d–Fig. 4f, Controller 3+PVC results in a higher overall γ and path velocity $\dot{s}$ than Controller 1–2+PVC. The path traversal time for Controller 3+PVC increases by only 3.5% compared to 14.3% and 9.1% for Controller 1–2+PVC, respectively (see Table III). The RMSE and $e_{\max}$

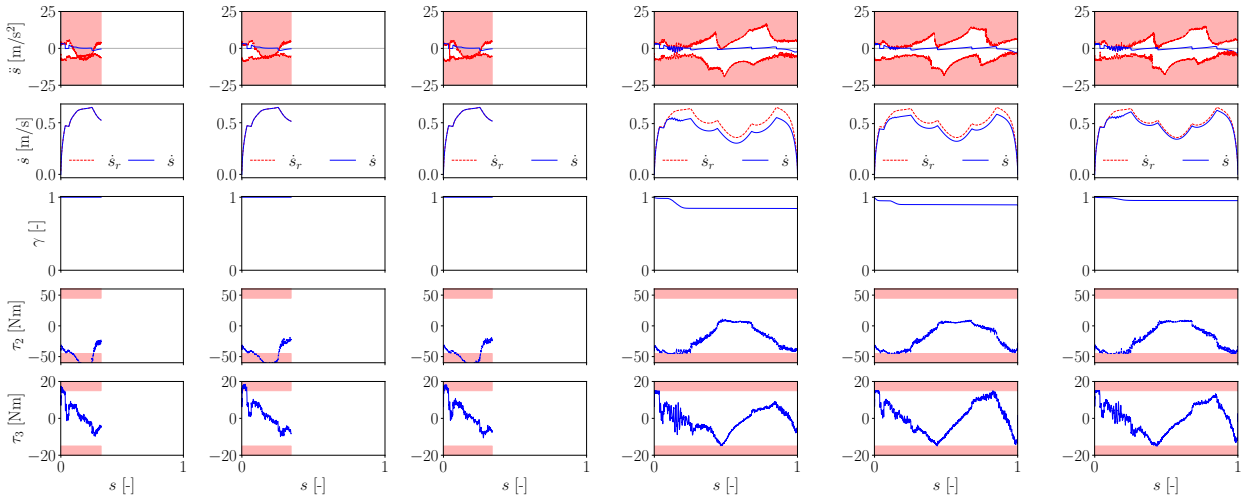

(a) Controller 1 (b) Controller 2 (c) Controller 3 (d) Controller 1+PVC (e) Controller 2+PVC (f) Controller 3+PVC

Fig. 4: Time-optimal path-tracking in experiments of a circular path under kinematic and dynamic uncertainties. In subplots (a)–(c), the experiments are stopped because of joint velocity limit violations. Within each subplot, the signals from top to bottom are path acceleration $\ddot{s}$, path velocity $\dot{s}$, joint torques τ_2 and τ_3. The red areas indicate inadmissible regions for signals.

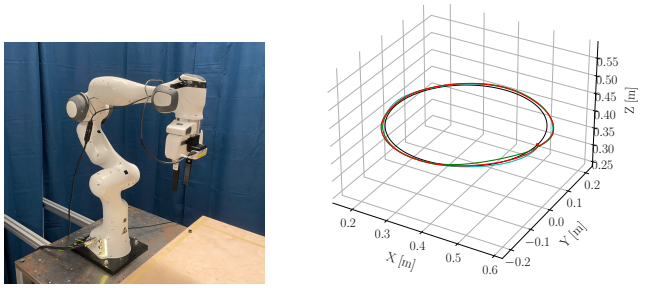

(a) Panda in experiments (b) Tool center point position

Fig. 5: Panda robot tracking a circular path in Cartesian space. The blue, green, and red solid lines represent the resulting positions with Controller 1+PVC, Controller 2+PVC, and Controller 3+PVC, respectively.

for both position and angle are comparable for Controller 1–3+PVC. Unlike in simulations, the torque constraint is satisfied by Controller 1+PVC in experiments. This may be attributed to the additional damping by joint friction.

B. Discussion

Results in simulations and experiments demonstrate that PVC can be applied to task-space controllers to improve trajectory feasibility. The redundancy can be utilized to further improve the performance by tracking time-optimal joint trajectories in nullspace, achieving shorter path traversal time while maintaining comparable or improved path-tracking accuracy. The reason why tracking the joint trajectory in nullspace implies higher performance may be because keeping the joint angles close to the inverse kinematics solution provides an approximate Jacobian to realize the nominal task-space motion. In addition, the nullspace and task-space motions can be fully coordinated when tracking the joint trajectory in (26). Despite not being the primary focus of this paper, both simulations and experiments indicate that tracking time-optimal joint trajectories in nullspace also reduces the risk of violating kinematic constraints.

TABLE III: Experimental results of time-optimal tracking of a circular path. Root Mean Squared Error for Position [mm] and Angle [rad], Maximum Path-Tracking Error for Position and Angle [rad], Path Traversal Time [s], Percent Increase [-] and Parameters.

Experiment	RMSE		$e_{\max}$		T	ΔP	α	k_γ	$\boldsymbol{K}_q$	$\boldsymbol{D}_q$
	Position	Angle	Position	Angle						
Controller 1+PVC	11.88	0.22	16.58	0.33	2.43	14.3%	20	50	100	20
Controller 2+PVC	13.71	0.19	22.93	0.33	2.32	9.1%	20	50	-	40
Controller 3+PVC	12.58	0.21	17.89	0.34	2.20	3.5%	20	5	400	40

VIII. Conclusions and Future Research

The performance of task-space path-velocity control for the time-optimal path-tracking problem with torque-limited redundant manipulators has been investigated and evaluated. Simulations and experiments demonstrate that task-space control performance can be significantly improved with the integration of path-velocity control, which dynamically scales the task-space motions for improved trajectory feasibility and path-tracking accuracy in the presence of uncertainties. Further improvements can be achieved by tracking the joint trajectory associated with the tasks in nullspace. Future work includes evaluating the performance with other task-space control methods and nullspace designs.

References

[1] R. Kelly, V. Santibáñez, and A. Loría, *Control of Robot Manipulators in Joint Space*. London: Springer-Verlag, 2005.

[2] C.-C. Cheah, C. Liu, and J.-J. E. Slotine, "Adaptive jacobian tracking control of robots with uncertainties in kinematic, dynamic and actuator models," *IEEE Transactions on Automatic Control*, vol. 51, no. 6, pp. 1024–1029, 2006.

[3] C.-C. Cheah, M. Hirano, S. Kawamura, and S. Arimoto, "Approximate jacobian control for robots with uncertain kinematics and dynamics," *IEEE Transactions on Robotics and Automation*, vol. 19, no. 4, pp. 692–702, 2003.

[4] T. Marcucci, C. Della Santina, M. Gabiccini, and A. Bicchi, "Towards minimum-information adaptive controllers for robot manipulators," in *2017 American Control Conference (ACC)*, pp. 4209–4214, IEEE, 2017.

[5] O. Dahl and L. Nielsen, "Torque-limited path following by online trajectory time scaling," *IEEE Transactions on Robotics and Automation*, vol. 6, no. 5, pp. 554–561, 1990.

[6] O. Dahl, "Path-constrained robot control with limited torques-Experimental evaluation," *IEEE Transactions on Robotics and Automation*, vol. 10, no. 5, pp. 658–669, 1994.

[7] O. Dahl, *Path Constrained Robot Control*. Thesis No. TFRT-1038, Department of Automatic Control, Lund University, 1992.

[8] B. Olofsson and L. Nielsen, "Path-tracking velocity control for robot manipulators with actuator constraints," *Mechatronics*, vol. 45, pp. 82–99, 2017.

[9] C. G. L. Bianco and O. Gerelli, "Online trajectory scaling for manipulators subject to high-order kinematic and dynamic constraints," *IEEE Transactions on Robotics*, vol. 27, no. 6, pp. 1144–1152, 2011.

[10] G. Antonelli, S. Chiaverini, and G. Fusco, "A new on-line algorithm for inverse kinematics of robot manipulators ensuring path tracking capability under joint limits," *IEEE Transactions on Robotics and Automation*, vol. 19, no. 1, pp. 162–167, 2003.

[11] J. M. Hollerbach, "Dynamic scaling of manipulator trajectories," in *1983 American Control Conference (ACC)*, pp. 752–756, IEEE, 1983.

[12] H. Sadeghian, L. Villani, M. Keshmiri, and B. Siciliano, "Task-space control of robot manipulators with null-space compliance," *IEEE Transactions on Robotics*, vol. 30, no. 2, pp. 493–506, 2013.

[13] Y. Nakamura, H. Hanafusa, and T. Yoshikawa, "Task-priority based redundancy control of robot manipulators," *The International Journal of Robotics Research*, vol. 6, no. 2, pp. 3–15, 1987.

[14] J. M. S. Ducaju, B. Olofsson, A. Robertsson, and R. Johansson, "Null-space compliance variation for safe human-robot collaboration in redundant manipulators using safety control barrier functions," in *2023 IEEE/RSJ International Conference on Intelligent Robots and Systems (IROS)*, pp. 5903–5909, IEEE, 2023.

[15] J. M. S. Ducaju, B. Olofsson, A. Robertsson, and R. Johansson, "Joint stiction avoidance with null-space motion in real-time model predictive control for redundant collaborative robots," in *2021 30th IEEE International Conference on Robot & Human Interactive Communication (RO-MAN)*, pp. 307–314, IEEE, 2021.

[16] S. Chiaverini, "Singularity-robust task-priority redundancy resolution for real-time kinematic control of robot manipulators," *IEEE Transactions on Robotics and Automation*, vol. 13, no. 3, pp. 398–410, 1997.

[17] M. W. Spong, S. Hutchinson, and M. Vidyasagar, *Robot Modeling and Control*, vol. 3. John Wieley & Sons, 2020.

[18] B. Siciliano, L. Sciavicco, L. Villani, and G. Oriolo, *Robotics: Modelling, Planning and Control*. London: Springer, 2009.

[19] J. E. Bobrow, S. Dubowsky, and J. S. Gibson, "Time-optimal control of robotic manipulators along specified paths," *The International Journal of Robotics Research*, vol. 4, no. 3, pp. 3–17, 1985.

[20] H. Pham and Q.-C. Pham, "A new approach to time-optimal path parameterization based on reachability analysis," *IEEE Transactions on Robotics*, vol. 34, no. 3, pp. 645–659, 2018.

[21] Z. Shiller and H.-H. Lu, "Computation of path constrained time optimal motions with dynamic singularities," *Journal of Dynamic Systems, Measurement, and Control*, vol. 114, pp. 34–40, 03 1992.

[22] K. Shin and N. McKay, "Selection of near-minimum time geometric paths for robotic manipulators," *IEEE Transactions on Automatic Control*, vol. 31, no. 6, pp. 501–511, 1986.

[23] D. Verscheure, B. Demeulenaere, J. Swevers, J. De Schutter, and M. Diehl, "Time-optimal path tracking for robots: A convex optimization approach," *IEEE Transactions on Automatic Control*, vol. 54, no. 10, pp. 2318–2327, 2009.

[24] Q.-C. Pham, "A general, fast, and robust implementation of the time-optimal path parameterization algorithm," *IEEE Transactions on Robotics*, vol. 30, no. 6, pp. 1533–1540, 2014.

[25] J. Nakanishi, R. Cory, M. Mistry, J. Peters, and S. Schaal, "Comparative experiments on task space control with redundancy resolution," in *2005 IEEE/RSJ International Conference on Intelligent Robots and Systems*, pp. 3901–3908, IEEE, 2005.

[26] C. Ott, *Cartesian impedance control of redundant and flexible-joint robots*. New York, NY, USA: Springer, 2008.

[27] O. Khatib, "A unified approach for motion and force control of robot manipulators: The operational space formulation," *IEEE Journal on Robotics and Automation*, vol. 3, no. 1, pp. 43–53, 1987.

[28] F. Caccavale, C. Natale, B. Siciliano, and L. Villani, "Six-dof impedance control based on angle/axis representations," *IEEE Transactions on Robotics and Automation*, vol. 15, no. 2, pp. 289–300, 1999.

[29] C. Gaz, M. Cognetti, A. Oliva, P. R. Giordano, and A. De Luca, "Dynamic identification of the Franka Emika Panda robot with retrieval of feasible parameters using penalty-based optimization," *IEEE Robotics and Automation Letters*, vol. 4, no. 4, pp. 4147–4154, 2019.

[30] P. Corke and J. Haviland, "Not your grandmother's toolbox–The robotics toolbox reinvented for python," in *2021 IEEE International Conference on Robotics and Automation (ICRA)*, pp. 11357–11363, IEEE, 2021.